Three-dimensional static speckle fields. Part I. Theory and numerical investigation

Dayan Li,[1] Damien P. Kelly,[2] and John T. Sheridan[1,*]

[1]*UCD Communications and Optoelectronic Research Centre, SFI-Strategic Research Cluster in Solar Energy Conversion, School of Electrical, Electronic and Mechanical Engineering, College of Engineering, Mathematical and Physical Sciences, University College Dublin, Belfield, Dublin 4, Ireland*

[2]*Institut für Mikro- und Nanotechnologien, Macro-Nano, Fachgebiet Optik Design, Technische Universität Ilmenau, Postfach 100565, 98684 Ilmenau, Germany.*

**Corresponding author: john.sheridan@ucd.ie*

Received June 15, 2011; accepted July 12, 2011;
posted July 25, 2011 (Doc. ID 149094); published August 25, 2011

When monochromatic light is scattered from an optically rough surface a complicated three-dimensional (3D) field is generated. These fields are often described by reference to the 3D volume (extent) of their speckles, leading to the definition of lateral (x, y) and longitudinal speckle sizes (z). For reasons of mathematical simplicity the longitudinal speckle size is often derived by examining the decorrelation of the speckle field for a single point lying on axis, i.e., $x = y = 0$, and this size is generally assumed to be representative for other speckles that lie further off-axis. Some recent theoretical results, however, indicate that in fact longitudinal speckle size gets smaller as the observation position moves to off-axis spatial locations. In this paper (Part I), we review the physical argument leading to this conclusion and support this analysis with a series of robust numerical simulations. We discuss, in some detail, computational issues that arise when simulating the propagation of speckle fields numerically, showing that the spectral method is not a suitable propagation algorithm when the autocorrelation of the scattering surface is assumed to be delta correlated. In Part II [J. Opt. Soc. Am. A **28**, 1904 (2011)] of this paper, experimental results are provided that exhibit the predicted variation of longitudinal speckle size as a function of position in x and y. The results are not only of theoretical interest but have practical implications, and in Part II a method for locating the optical system axis is proposed and experimentally demonstrated.

OCIS codes: 030.6140, 030.6600, 050.1940, 070.7345, 200.2610.

1. INTRODUCTION

A three-dimensional (3D) speckle field is produced when an optically rough surface is illuminated by coherent laser light. Statistical properties of the resultant speckle fields are usually examined by studying the space-time cross-correlation function in the observation plane that is perpendicular to the optical axis. In 1981, Ohtsubo [1] systematically discussed the time-space cross-correlation function of dynamic speckles produced by a moving diffuse object under Gaussian beam illumination. Later, a useful review of the statistical properties of dynamic speckles was presented by Yoshimura [2], in which other illumination conditions were also examined. Essentially, these papers concentrated on investigating the time and spatial (x and y only) properties of speckles in the observation plane. In 1990, Leushacke and Kirchner [3] examined the 3D structure of static speckle under plane wave illumination. Li and Chiang [4] also investigated 3D speckle and measured the lateral and on-axis longitudinal speckle size, respectively, by examining the diffraction halos and the Young's fringes of the specklegrams. Later, the 3D space-time cross-correlation function for free-space geometry under Gaussian beam illumination was presented by Yoshimura and Iwamoto [5]. In 1999, the work in [5] was extended by Yura *et al.* [6] to include other paraxial optical systems and soft Gaussian apertures using the ABCD matrix theory with complex values for the system parameters. Recently, a generalized Yamaguchi correlation factor was derived using the Linear Canonical Transform and the associated ABCD matrix theory for a hard limiting aperture [7,8]. Such methods have been shown to be of great convenience when examining speckle size and controlling speckle characteristics in various paraxial optical systems [9–15].

The 3D average speckle sizes are critical parameters in laser speckle metrology and laser holographic interferometry. However, as noted in [4], no consistent experimental results on the longitudinal speckle size were reported while photosensitive films were being used as the recording materials [16,17]. Two critical assumptions have typically been made when deriving these physical models: (i) the scattered fields on the diffuser surface are delta correlated, and (ii) the speckle fields in the observation plane obey a complex Gaussian random process. Digital cameras (CCDs) are now widely used to record speckle patterns, which greatly simplifies the experimental procedure for testing the validity of these approximations. Nevertheless, experimental investigations of the longitudinal speckle correlation properties are relatively rare compared with the numerous theoretical models that have been developed based on these assumptions [3–5,13,18–20].

Using these assumptions, it is possible to derive a correlation function describing the statistical relationship of the speckle fields at two different point positions. Naturally, if the two point positions coincide (i.e., we compare the intensity at a point to itself), we find a normalized correlation value

of unity. As these points become further separated from each other, the correlation value tends to decrease. Two points are said to be totally decorrelated when this correlation function decreases to zero, and indeed this is often used to define the lateral and longitudinal speckle size [4]. For numerical and experimental purpose, the average speckle size in a particular direction is often defined as the distance at which the correlation function takes the value of 0.5 [3].

In this two part paper we first numerically (Part I) and second experimentally (Part II [21]) determine this correlation function and compare it to the predictions of the appropriate physical model. We note that performing such a comparison is not straightforward. The correlation function is mathematically represented by the ensemble average of the intensity values at the two point positions, which can be realized either by time averaging or by space averaging depending on the experimental conditions, i.e., where the generated speckle fields are assumed to be approximately ergodic [22,23]. To illustrate the issues involved assume we have a speckle field generated with a diffuser and a monochromatic light source. After recording the resulting intensities for the two point positions, the original diffuser is replaced with a second one (we assume that the second diffuser has statistically similar surface roughness characteristics) and the measurement is repeated. It is highly probable that different intensity values will be recorded. If we proceed in this manner, changing diffusers and making measurements at the same two point positions, we will build up two data vectors corresponding to the series of intensities recorded at the two points. Once reasonably large datasets have been recorded (>1000 values), the resulting correlation function for these two points can be experimentally estimated by cross-correlating the two data vectors (the mean of each vector being first subtracted from the vector before a normalized cross correlation is performed). This approach is however rather slow, therefore, in this manuscript we replace this form of "time averaging" with a "spatial averaging" [23,24], where for a single diffuser we take intensity values around the two points of interest and use these values to determine the value of the correlation function. While this approximation is not strictly true, our numerical simulations and experimental results (which involve spatial averaging) have been found to be consistent with the prediction of the physical model (involving the use of the ensemble average). Therefore, this approximation broadly holds for the static free-space speckles we are investigating here.

In [25] the authors present a new theoretical model for the description of speckle fields. The model predicts a series of interesting speckle characteristics (in three different regimes) that are demonstrated experimentally in a follow-up paper [26]. In this model the input field is assumed to be factorized into two well-separated spatial variations: one describes the lateral average speckle size and the other is the lateral size of the illuminating spot in the input plane. The input field is no longer assumed to be delta correlated (in the input plane) as is the case for the model examined here. However, the input field in [25] can be considered as being generated by a delta correlated field which then propagates a specific longitudinal distance z_0 to the input plane. As a result, identical speckle characteristics are predicted by the authors of [25] (in the Van Cittert–Zernike regime), and by us (calculated for the Fresnel regime), when equivalent propagation distances are used, i.e., see Eq. (41) in [25] and Eq. (11) below. Our work differs from that presented in [25,26], as we examine numerical simulations and off-axis and longitudinal speckle field characteristics.

In this paper we begin by closely examining the 3D decorrelation properties of speckle patterns. The relation between the correlation coefficients obtained for each discrete sample position and the analytic predictions at the corresponding spatial position are also clarified. We then describe a numerical technique, employing the standard direct method (DM) [27–29], to accurately simulate the propagation of the speckle fields in the Fresnel regime. The decorrelation trends predicted by the analytic expressions for both in-plane and out-of-plane displaced speckle fields are reproduced using our simulated speckle patterns. Therefore, a numerical approach, which can simulate the physical situation, is provided. The term in-plane (or lateral) refers to the directions that are perpendicular to the optical axis, while out-of-plane (or longitudinal) describes directions parallel to the optical axis. Based on our studies we note that an alternative algorithm for simulation field propagation, the spectral method (SM) [27–29], is not suitable for simulating longitudinally displaced speckle patterns when a delta correlated input field is assumed. This appears to be due to the way in which the fast Fourier transform (FFT) is used to implement the SM algorithm, and this is discussed later in Section 3.

In Part II [21], we present accurate experimental measurements to determine the resulting correlation coefficients. The variation of the decorrelation function with respect to off-axis position is specifically examined, leading to a novel optical axis identification and alignment technique. As a result, the well-known physical model for fully developed speckle is more clearly understood and more accurately verified.

The layout of Part I of this paper is as follows: building on the work in [3,5], in Subsection 2.A, we first rederive an analytic space correlation function describing the statistical relationship at two different point positions in a speckle field. This expression predicts important properties (decorrelation trends) for speckle in 3D, which are presented in Subsection 2.B. In Section 3, a discrete correlation algorithm, which is based on area speckle patterns, is described and used. The resulting correlation coefficients obtained at each sample position are shown to be closely related to the corresponding analytic predictions. The decorrelation trends described in Subsection 2.B are simulated in Subsection 3.B using the DM, and it is shown that the SM is not a suitable algorithm for our simulations. Finally, in Section 4, we present some concluding remarks.

2. 3D SPECKLE CORRELATION FUNCTION

A. Theory

In this section we briefly review the derivation of the 3D speckle correlation function. The free-space optical setup is shown in Fig. 1. A diffuser is placed in the object plane (ξ, η) and illuminated from behind with monochromatic light of wavelength λ. In our analysis we examine two situations: when the extent of the object plane is limited by (i) a hard circular aperture of diameter $2w$ or (ii) a soft Gaussian aperture with an effective extent of $2w$. The scattered light propagates to the observation plane (x, y), where the speckle intensity pattern is recorded by a camera, located a distance

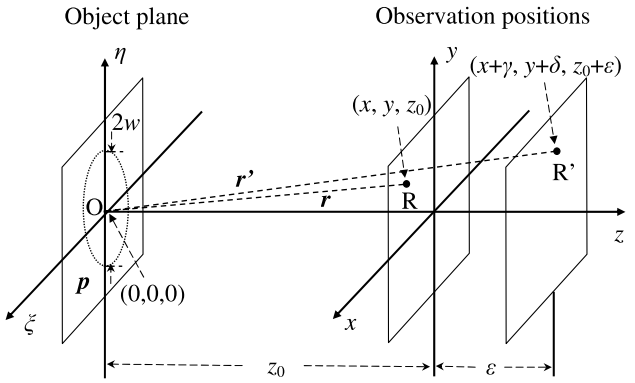

Fig. 1. Free-space propagation geometry for static speckle formation. The illuminating spot on the diffuse object is circular with diameter $2w$.

z_0 from the object plane. Here we restrict our attention to fully developed speckle formed when the surface roughness exceeds the wavelength of the illuminating light and where the surface correlation extent is much smaller than the illuminated area. If a sufficiently large number of independent scattering points within this aperture contribute to form the speckle field, then by adopting the central limit theorem [30,31], the resultant field in the observation plane obeys a complex Gaussian random process. Note that in this manuscript we assume that the diffuser randomly modulates the phase of the incident beam and that the amplitude of the illuminating wave field, just before and just after the diffuser, is not changed. Although this does not satisfy the requirements identified by Goodman [18] (see Chapter 2, p. 8), since the real and imaginary parts of the complex amplitude are supposed to be statistically independent, we have found from extensive simulations that the resulting distribution in the observation plane still follows a Gaussian random process.

We now wish to compare statistically the speckle intensities, $I(\boldsymbol{r}) = A(\boldsymbol{r})A^*(\boldsymbol{r})$ and $I(\boldsymbol{r}') = A(\boldsymbol{r}')A^*(\boldsymbol{r}')$, at point positions $\boldsymbol{r}$ and $\boldsymbol{r}'$, and so we calculate the ensemble average. Since the intensity distributions obey a random Gaussian process, we can reduce the complexity of this equation using Reeds theorem [31], so that

$$\begin{aligned}\langle I(\boldsymbol{r})I(\boldsymbol{r}')\rangle &= \langle A(\boldsymbol{r})A^*(\boldsymbol{r})A(\boldsymbol{r})A^*(\boldsymbol{r}')\rangle,\\ \langle I(\boldsymbol{r})I(\boldsymbol{r}')\rangle &= \langle I(\boldsymbol{r})\rangle\langle I(\boldsymbol{r}')\rangle + |\langle A(\boldsymbol{r})A^*(\boldsymbol{r}')\rangle|^2,\end{aligned} \tag{1}$$

where $\langle\cdots\rangle$ indicates an ensemble average and the star denotes complex conjugation. The first two terms in Eq. (1) are the mean intensity of the speckle patterns. The normalized correlation function of intensity is given by

$$\frac{\langle I(\boldsymbol{r})I(\boldsymbol{r}')\rangle}{\langle I(\boldsymbol{r})\rangle\langle I(\boldsymbol{r}')\rangle} = 1 + |\mu_{12}(\boldsymbol{r},\boldsymbol{r}')|^2, \tag{2}$$

where the normalized mutual intensity, μ_{12}, is defined as

$$\mu_{12}(\boldsymbol{r},\boldsymbol{r}') = \frac{\langle A(\boldsymbol{r})A^*(\boldsymbol{r}')\rangle}{[\langle A(\boldsymbol{r})A^*(\boldsymbol{r})\rangle\langle A(\boldsymbol{r}')A^*(\boldsymbol{r}')\rangle]^{1/2}}. \tag{3}$$

The square modulus of the normalized mutual intensity is sufficient to describe the correlation of intensity. In the speckle literature, $|\mu_{12}|^2$ is usually referred to as the correlation coefficient of intensity [3].

Denoting the complex amplitude of the incident field in the object plane by $A_0(\boldsymbol{p})$, the optical field at position $\boldsymbol{r}$ in the observation plane is given using the Rayleigh–Sommerfeld formula by

$$A(\boldsymbol{r}) = \frac{1}{i\lambda}\iint A_0(\boldsymbol{p})\frac{z_0}{|\boldsymbol{r}-\boldsymbol{p}|}\frac{\exp(ik|\boldsymbol{r}-\boldsymbol{p}|)}{|\boldsymbol{r}-\boldsymbol{p}|}\mathrm{d}\xi\mathrm{d}\eta, \tag{4}$$

where integration is carried out over the entire illuminated area and $|\boldsymbol{r}-\boldsymbol{p}| = \sqrt{(x-\xi)^2+(y-\eta)^2+z_0^2}$, as illustrated in Fig. 1. Applying Eq. (4), it can be shown that the cross correlation of the field at the two points $\boldsymbol{r}$ and $\boldsymbol{r}'$ is giving by

$$\begin{aligned}\langle A(\boldsymbol{r})A^*(\boldsymbol{r}')\rangle = \left(\frac{z}{\lambda}\right)^2 \iint\iint \langle A_0(\boldsymbol{p}_1)A_0^*(\boldsymbol{p}_2)\rangle\\ \frac{\exp[ik(|\boldsymbol{r}-\boldsymbol{p}_1|-|\boldsymbol{r}'-\boldsymbol{p}_2|)]}{|\boldsymbol{r}-\boldsymbol{p}_1|^2|\boldsymbol{r}'-\boldsymbol{p}_2|^2}\mathrm{d}\xi_1\mathrm{d}\eta_1\mathrm{d}\xi_2\mathrm{d}\eta_2.\end{aligned} \tag{5}$$

Here we apply the assumption that the field just in the object plane is delta correlated, and hence we write

$$\langle A_0(\boldsymbol{p}_1)A_0^*(\boldsymbol{p}_2)\rangle = C_0E(\boldsymbol{p}_1)E^*(\boldsymbol{p}_2)\delta(\boldsymbol{p}_1-\boldsymbol{p}_2), \tag{6}$$

where C_0 is a constant and $E(\boldsymbol{p})$ represents the illuminating wave amplitude. $E(\boldsymbol{p})$ is used as it has been assumed that the microscopic structure of the object only changes the phase of the incident light. Using Eq. (6), Eq. (5) simplifies to

$$\langle A(\boldsymbol{r})A^*(\boldsymbol{r}')\rangle = C_0\left(\frac{z}{\lambda}\right)^2\iint |E(\boldsymbol{p})|^2\frac{\exp[ik(|\boldsymbol{r}-\boldsymbol{p}|-|\boldsymbol{r}'-\boldsymbol{p}|)]}{|\boldsymbol{r}-\boldsymbol{p}|^2|\boldsymbol{r}'-\boldsymbol{p}|^2}\mathrm{d}\xi\mathrm{d}\eta. \tag{7}$$

Making the usual approximation to the denominator of the integrand in Eq. (7), i.e., $|\boldsymbol{r}-\boldsymbol{p}|^2 \approx |\boldsymbol{r}'-\boldsymbol{p}|^2 \approx z_0$, and normalizing as in Eq. (3), gives the desired expression for the square modulus of the normalized mutual intensity

$$|\mu_{12}(\boldsymbol{r},\boldsymbol{r}')|^2 = \left|\frac{\iint |E(\boldsymbol{p})|^2\exp[ik(|\boldsymbol{r}-\boldsymbol{p}|-|\boldsymbol{r}'-\boldsymbol{p}|)]\mathrm{d}\xi\mathrm{d}\eta}{\iint |E(\boldsymbol{p})|^2\mathrm{d}\xi\mathrm{d}\eta}\right|^2. \tag{8}$$

Examining Eq. (8),it can be seen that $|\mu_{12}|^2$ depends on the intensity distribution of the illuminating beam, the shape, and size of the illuminating spot on the object and the observation positions $(\boldsymbol{r},\boldsymbol{r}')$ with respect to the origin, $O=(0,0,0)$, which is defined by the location of the center of the illuminating spot. We compare the cases of plane wave and Gaussian beam illuminations by making the appropriate substitutions for $|E(\boldsymbol{p})|$.

For plane wave illumination, $|E(\boldsymbol{p})|$ is constant when $|\boldsymbol{p}| \le w$ and zero otherwise. To proceed, we simplify the expression in Eq. (8), by first making the Fresnel approximation to the exponent of the integrand [32] and then integrating over the area of the circular aperture. The expression for $|\mu_{12}|^2$, between field at point positions $R=(x,y,z_0)$ and $R'=(x+\gamma,y+\delta,z_0+\varepsilon)$, as indicated in Fig. 1, is giving by [3]

$$|\mu_{12}(x,y,z_0;\gamma,\delta,\varepsilon)|^2 = \left|2\sum_{n=0}^{\infty} i^n(2n+1)j_n(u/4)J_{2n+1}(v)/v\right|^2, \tag{9}$$

where $u = -w^2\varepsilon k/z_0^2$, $v = wk\sqrt{(z_0\gamma - \varepsilon x)^2 + (z_0\delta - \varepsilon y)^2}/z_0^2$, and $k = 2\pi/\lambda$. j_n are the spherical Bessel functions and J_n are the Bessel functions of the first kind.

For Gaussian beam illumination, we define [5,33]

$$|E(\boldsymbol{p})| = \left(\frac{w_0}{w}\right)^2 \exp\left(-\frac{|\boldsymbol{p}|^2}{w^2}\right), \tag{10}$$

where w is the radius at which the beam amplitude drops to $1/e$ of the axial value in the object plane, and w_0 is a constant denoting the beam waist size. Making the Fresnel approximation to the exponent of the integrand in Eq. (8), and noting that in this case the integration is carried out over infinity, the expression for $|\mu_{12}|^2$ is given by [5]

$$|\mu_{12}(x,y,z_0;\gamma,\delta,\varepsilon)|^2 = \frac{1}{1+(\varepsilon/l_z)^2}\exp\left\{-\left(\frac{1}{r_s}\right)^2\left[\left(\frac{\varepsilon}{z_0}x-\gamma\right)^2 + \left(\frac{\varepsilon}{z_0}y-\delta\right)^2\right]\right\}, \tag{11}$$

where $l_z = 4z_0(z_0+\varepsilon)/(w^2k)$ and $r_s = 2(z_0+\varepsilon)[1+(\varepsilon/l_z)^2]^{1/2}/(wk)$.

Thus the speckle correlation coefficient for any two points in the 3D space can be determined using Eq. (9) for plane wave and Eq. (11) for Gaussian beam illumination.

B. Interpretation

The analytic expressions for $|\mu_{12}|^2$ indicate that speckle has 3D structure. In general, $|\mu_{12}|^2$ decreases as the spatial separation of the two correlating positions increases. We proceed by examining the predictions of Eq. (9) and (11), identifying the statistical properties as well as the average speckle size in a specific direction. Let us assume that we are examining the correlation between two points, $(x,0,z_0)$ and $(x+\gamma,0,z_0+\varepsilon)$ so that we can, for the moment, ignore the variable y. Under these conditions, we can make several observations.

I. If $\varepsilon \to 0$ and $\gamma \to 0$ then $|\mu_{12}|^2 = 1$, indicating 100% correlation for a speckle field correlated with itself.

II. If $\varepsilon \to 0$, we find that any decorrelation will be dependent on the variable γ only, i.e., the decorrelation does not depend on the spatial location in x and y. This is consistent with the analysis presented in [3–6,13].

III. For a fixed value of ε, $|\mu_{12}|^2$ gives equivalent correlation coefficients in the directions that pass through the system origin. As a result, in a specific observation plane, i.e., the $z = z_0$ plane, the speckles are oriented toward the system origin and have on average the same projection length onto the optical axis [3,5]. We now consider the correlation coefficients between the fields at point positions, see Fig. 2, which are divided into three groups: (i) Q_0 and Q_0' (located at the optical axis), (ii) Q_1 and Q_1'' (located on a straight line that passes through the system origin), and (iii) Q_2 and Q_2'' (located on a different line through the origin). Note that Q_0, Q_1, and Q_2 are all in the $z = z_0$ plane, while Q_0', Q_1'', and Q_2'' are located in the $z = z_0 + \varepsilon$ plane. Significantly, the $|\mu_{12}|^2$ values for the three groups are all equal. If it is assumed that in each of these three cases $|\mu_{12}|^2 = 0.5$, then the average speckle grain sizes along each of these three directions (the actual distance between the two points) has been found. In Fig. 2, an on-axis speckle grain and two off-axis grains are drawn. It is clear that

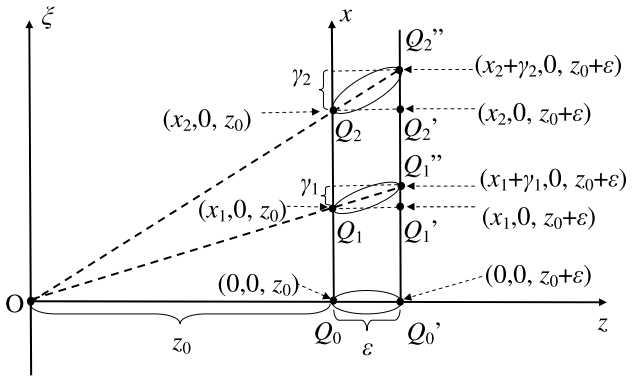

Fig. 2. Illustration in the x-o-z plane of the orientation property of the static speckle grains. In the figure, an on-axis speckle and two off-axis speckles have been drawn (three ellipses). The off-axis speckle sizes in the directions that pass through the system origin (denoted by dashed lines) have on average the same projection length onto the optical axis (z).

the further the position away from the optical axis, the larger the speckle size will be in the direction along the line that passes through the system origin. However, significantly, they all have the same projection length (ε) on the z axis, and this length is the on-axis speckle size.

IV. For a fixed value of ε, it can be seen that $|\mu_{12}|^2$ is maximized by ensuring that $\varepsilon(x/z_0) - \gamma = 0$. Thus when $x \neq 0$, a maximum correlation value is found when the second point is shifted in x by

$$\gamma = \varepsilon\left(\frac{x}{z_0}\right). \tag{12}$$

Figures 3(a) and 3(b) (solid curves) are plots of the analytic $|\mu_{12}(x_1,0,z_0;\gamma,\varepsilon)|^2$ values as a function of γ (the lateral shift in the x direction from Q_1) for plane wave and Gaussian beam illumination, respectively. The off-axis position in the $z = z_0$ plane is $Q_1 = (x_1,0,z_0)$. Choosing the longitudinal position Q_1' in the $z = z_0 + \varepsilon$ plane as the plot origin, which corresponds to $\gamma = 0$, position shifting of the peak correlation coefficient is observed. Some typical experimental values are chosen for the parameters used to generate Fig. 3: $\lambda = 633\,\text{nm}$, $w = 1.5\,\text{mm}$, $z_0 = 400\,\text{mm}$, $x_1 = 3.55\,\text{mm}$, and $\varepsilon = 0$, 5, 10, and 15 mm. ($\varepsilon = 0\,\text{mm}$ corresponds to the autocorrelation of the off-axis speckle field). The plots in Figs. 3(a) and 3(b) also show how the position of the peak correlation coefficient shifts in proportion to ε. We also note, however, that the peak value decreases as ε increases.

Equation (12) indicates that the out-of-plane displacement of the diffuser can be estimated in the observation plane using the off-axis speckle correlation values, by substituting the longitudinal camera displacement ε with the out-of-plane displacement of the object surface, while keeping the camera position steady. The quantitative relationship between the parameters in the equation is verified experimentally in Part II [21].

Based on these results we therefore can conclude that position shifting of the peak correlation coefficient will occur when an off-axis speckle field is correlated with the fields (point fields) from a longitudinally displaced plane. The offset of the position in the x direction results in the peak correlation coefficient shifting by γ, while the offset of the position in the y direction results in the peak correlation coefficient shifting by δ (the lateral shift in the y axis). The cross correlation of an

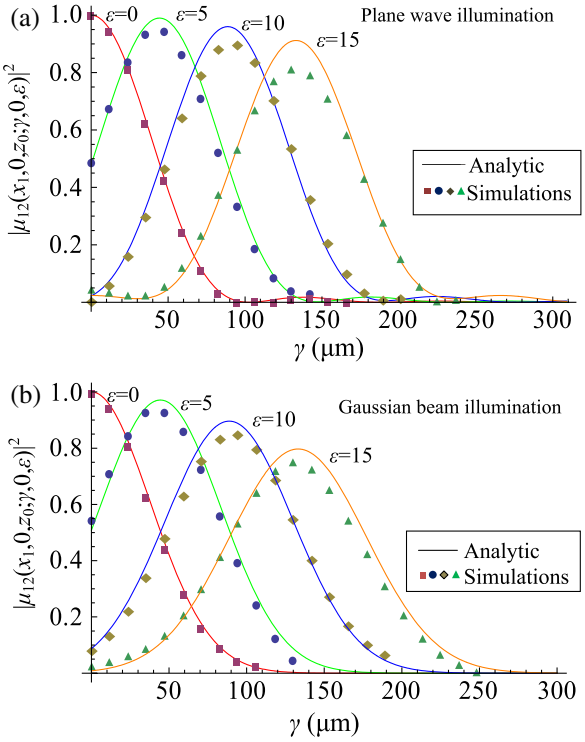

Fig. 3. (Color online) Lateral speckle correlation coefficients between an off-axis field at position $Q_1 = (x_1, 0, z_0)$ in the $z = z_0$ plane and fields in a longitudinally displaced plane $z = z_0 + \varepsilon$ (mm), as a function of γ. (a) Plane wave illumination. (b) Gaussian beam illumination.

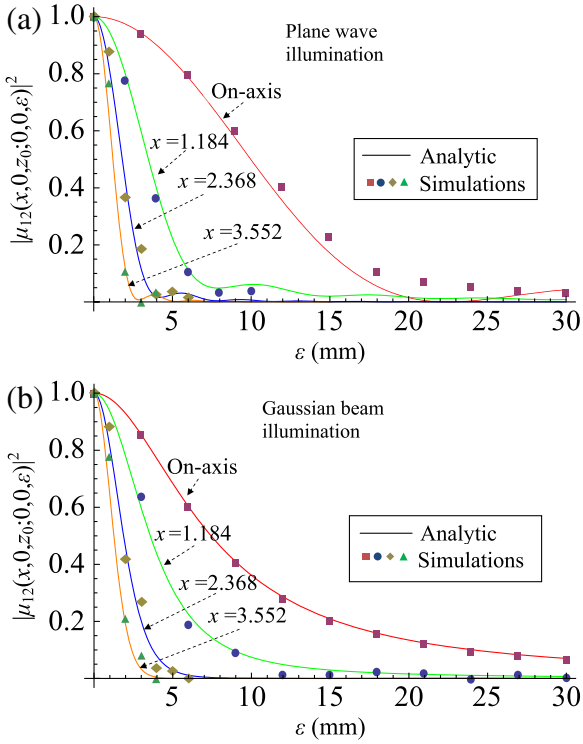

Fig. 4. (Color online) Longitudinal speckle correlation coefficients between the field at $Q = (x, 0, z_0)$ in the $z = z_0$ plane and a longitudinally displaced field in plane $z = z_0 + \varepsilon$, as a function of ε. x is in units of millimeters. (a) Plane wave illumination. (b) Gaussian beam illumination.

on-axis fields ($x = 0$), and the autocorrelation of an off-axis field ($\varepsilon = 0$), will produce the maximum coefficient value located at the origin, i.e., with zero shift.

V. If $\gamma = 0$ while the value of ε varies, longitudinal decorrelation of the speckle field takes place. Both on-axis ($x = 0$) and off-axis ($x \neq 0$) longitudinal decorrelation behavior, i.e., $|\mu_{12}(x, 0, z_0; 0, 0, \varepsilon)|^2$, as a function of ε are shown in Figs. 4(a) and 4(b) (solid curves) for the plane wave and Gaussian beam illumination, respectively. In order to observe the total decorrelation trends, while not breaking the Fresnel approximation requirement (i.e., $z_0 \gg \varepsilon$ when total decorrelation occurs), we set $z_0 = 200$ mm. The other parameter values are all identical to those used to generate Fig. 3. The results in Fig. 4 indicate that the longitudinal correlation coefficients of the off-axis fields decrease much more rapidly than those for on-axis, and the further one is away from the optical axis, the larger the decorelation rate is. This means that the off-axis longitudinal speckle size is much smaller than the on-axis longitudinal speckle size, and the off-axis longitudinal speckle size decreases dramatically as the point in the field examined is positioned further away in (x, y) from the optical axis.

VI. If $\gamma = 0$, $|\mu_{12}|^2$ is inversely proportional to x for a fixed value of ε. This can be inferred based on the results presented above. To illustrate this property, $|\mu_{12}(r, z_0; 0, 0, \varepsilon)|^2$ is plotted as a function of the offset r (where $r = \sqrt{x^2 + y^2}$), see Fig. 5. The parameter values used are $w = 1.5$ mm, $z_0 = 200$ mm, and $\varepsilon = 5$ mm. The two longitudinally displaced speckle patterns in the observation planes $z = z_0$ and $z = z_0 + \varepsilon$, produce a monotonically decreasing longitudinal correlation coefficient along the radial direction. (Some small fluctuations can be observed to occur for plane wave illumination in the region where r is larger enough that the total decorrelation takes place). This property can be applied to locate the optical axis in relation to the camera center, which is demonstrated in Part II [21].

3. DISCRETE CORRELATION ALGORITHM AND NUMERICAL SIMULATIONS

As indicated in Section 2, the derived expressions for $|\mu_{12}|^2$ are continuous functions. Theoretically, the correlation between fields at any two different point positions in the free-space Fresnel regime can be found using Eq. (9) or (11) as discussed. However, in practice the measured speckle fields are discrete values corresponding to the total light intensity incident on each camera element area (i.e., camera pixels). Furthermore, the derivation of the analytic correlation is

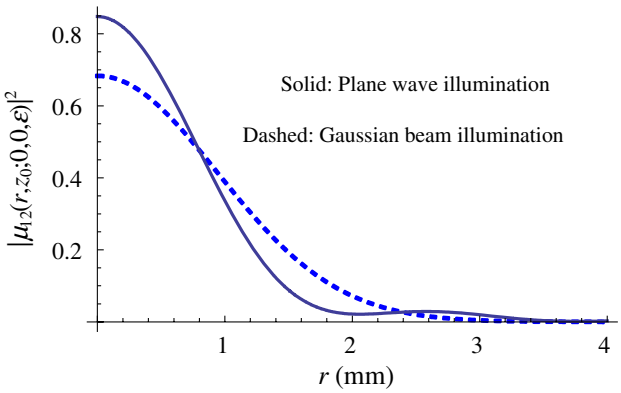

Fig. 5. (Color online) Longitudinal speckle decorrelation as a function of radial offset r, between fields from two longitudinally displaced planes $z = z_0$ and $z = z_0 + \varepsilon$.

based on ensemble averaging of the fields at point positions, which are time consuming and difficult to realize in practice. In this section, we briefly describe a discrete correlation algorithm that can be used to calculate the speckle correlation coefficients. This algorithm uses two discrete speckle images to compute the correlation coefficient for fields at the image center. As a result, spatial averaging is used instead of the ensemble time average when calculating the speckle correlation coefficients. We reiterate that this substitution is appropriate and the obtained discrete correlation coefficients can be directly related to the analytic predictions at each sample position. Next, the standard DM is used to calculate the propagation of the speckle fields in the Fresnel regime. The discrete correlation algorithm is applied to the resulting simulated speckle images, and the decorrelation trends discussed in Section 2 are accurately reproduced. Therefore, a verified numerical simulation method, which agrees with the predictions of the standard physical model of fully developed speckle, is provided.

A. Discrete Correlation Algorithm

The core command we have used to perform the two-dimensional speckle correlation is the MATLAB in-built function "normxcorr2" [34]. Consider two discrete speckle images $f(m,n)$ and $t(m,n)$ with image array sizes of m and n in the two dimensions. The algorithm used to compute the normalized correlation coefficients is given by the following formula:

$$c(g,l)=\frac{\sum_{m,n}[f(m,n)-\bar{f}_{g,l}][t(m-g,n-l)-\bar{t}]}{\left\{\sum_{m,n}[f(m,n)-\bar{f}_{g,l}]^2\sum_{m,n}[t(m-g,n-l)-\bar{t}]^2\right\}^{1/2}}, \quad (13)$$

where $\bar{t}$ is the mean of $t(m,n)$ and $\bar{f}_{g,l}$ is the mean of the part of $f(m,n)$ overlapping the second image $t(m,n)$ during the calculation of each correlation value, $c(g,l)$.

This algorithm first shifts the second image $t(m,n)$ a distance g (or l) in the x (or y) direction, and a cross-correlation coefficient between the fields at sample positions $(m/2, n/2)$ and $(m/2-g, n/2-l)$ is calculated by summing all the product values for all the overlapping sample elements. The normalization of the cross-correlation coefficient is then carried out. Note that the spatial average factor, $1/(m\times n)$, in both the numerator and denominator of Eq. (13), has been canceled out. Therefore, this algorithm is a spatially averaging approach, which uses area speckle images to calculate correlation coefficients for point positions. Following the terminology in [5], we define the center of the first image $(m/2, n/2)$ to be the standard observation position (SOP). Examining the correlation algorithm, we note that it returns the speckle correlation coefficients between the field at the SOP and the fields at the sample positions of the second image. In other words, $c(g,l)$ is the correlation coefficient between the field at the SOP and the field at the sample position $(m/2-g, n/2-l)$ in the second image, which is (g,l) distance away from the center of the second image. In order to validate the algorithm in the next section we simulate area speckle images and compare the numerically obtained correlation coefficients with the analytic predictions.

B. Numerical Simulations

In this section we wish to examine, from a numerical perspective, issues that arise when propagating a field, with a random phase uniformly distributed over 2π [3], over a given distance of free space. Two standard free-space propagation algorithms, the DM and the SM, are used to calculate the speckle images in the observation plane. As will be seen, while the DM works well, the SM is not suitable to simulate the results for longitudinally displaced speckle images.

A square matrix of dimension $N\times N$ is used to describe the input field immediately in front of the diffuser, i.e., the object plane in Fig. 1. Within this square matrix, a subarray of "circular diameter" C samples is used to model the finite extent of the illuminating field on the object surface. This sample number C is given by $C=2w/\Delta\xi$, where $\Delta\xi$ is the sampling period in the object plane. The amplitudes of the complex numbers in the array are generated from the magnitude of the illuminating distribution, while a pseudorandom number generator is used to generate uniformly distributed phase values over the interval $[0-2\pi]$. As an example consider the case of plane wave illumination: in this case the discrete amplitudes values outside the circular subarray are set to zero, while those inside to unity. When we consider Gaussian illumination, we turn to Eq. (10) to generate all the matrix values. The matrix is then Fresnel transformed using an FFT-based algorithm (DM or SM) in order to calculate Eq. (4). In this way the desired output field and the speckle intensity in the observation plane are generated.

An important difference between the DM and SM algorithms is the number of FFT operations that need to be performed. For the DM, only one FFT operation is carried out. Because of the nature of the FFT algorithm, this leads to a scaling in the output plane where the input sample interval $\Delta\xi$ maps to the output sample interval Δx according to the following relationship:

$$\Delta x=\frac{\lambda z_0}{N\Delta\xi}. \quad (14)$$

On the other hand for the SM, where two FFT operations are carried out, the scale factor is canceled out between the two FFT operations. Therefore, for the SM, the sample interval Δx remains constant, i.e., $\Delta x=\Delta\xi$.

In the simulation of longitudinally displaced speckle images, Δx is an important parameter. We first use the DM for our simulation. Equation (14) indicates that the sample interval Δx of the simulated image depends on N. As a result, by choosing a suitable value of N, the ratio of Δx to the average lateral speckle size in the observation plane $z=z_0$ can be controlled. When $N=C$, there is on average only one speckle grain at each matrix element due to the fact that the lateral average speckle size in plane $z=z_0$ is $\lambda z_0/(2w)$. When $N>C$, the field in the object plane is zero padded before Fresnel transformation (propagating to the observation plane). As a result, we can examine in finer detail the distribution in the output plane. In the simulation, we choose $N>C$, so that on average one speckle grain will cover several matrix elements. This represents the experimental situation where w and z_0 are appropriately chosen to make sure that in the observation plane the lateral speckle size is several times larger than the camera pixel size. In order to compare the simulating results and the analytic prediction, knowledge of the Δx value is

necessary. The relationship between the sample intervals in the object plane and in the observation plane, Δx, is given by Eq. (14). Given the close agreement between the analytic and numerical results presented in Figs. 3 and 4, the predictions of Eq. (14) have been verified.

We now simulate the lateral decorrelation trends. Four speckle patterns in different observation planes $z_0 + \varepsilon$ ($\varepsilon = 0$, 5, 10, and 15 mm) are generated. It should be noted that these simulated speckle patterns have different sample interval values Δx in each of the four observation planes, as indicated by Eq. (14). As a result, in order to simulate the speckle patterns captured by a camera placed in these observation planes, the number of samples in the last three patterns must be increased by a factor of $(z_0 + \varepsilon)/z_0$. This task can be carried out using the in-built MATLAB function "imresize" [35], which resamples and interpolates the pattern according to the given rescaling factor. After the resizing operation, the sample interval value Δx of the four speckle patterns can be considered the same. We choose $N = 1000$, $\Delta\xi = 21.38\,\mu$m, $w = 1.5$ mm, $z_0 = 400$ mm, and $\lambda = 633$ nm. As a result, after resizing, the sample interval of the four simulated patterns is 11.84 μm. Then four image subsets, containing 200×200 samples, centered at (300, 0) away from the image center, are selected from the four images. This means that the subsets are all the same size and are all centered in the same transversal region with respect to the optical axis, i.e., the SOP is (3.55 mm, 0). Correlation operations are performed, using the discrete correlation algorithm, between the first and each of the other three subset images. The resulting correlation coefficients estimated from simulating both plane waves, in Fig. 3(a), and Gaussian beam illumination, in Fig. 3(b), are compared with the corresponding analytic predictions.

Next, we simulate longitudinal decorrelation effects. We ensure the validity of the Fresnel transform by ensuring that $z_0 \gg \varepsilon$, setting $z_0 = 200$ mm and $\Delta\xi = 10.69\,\mu$m in this simulation. The other parameters used, i.e., N, w, and λ have the same values as used in the lateral case. Therefore, the sample interval Δx of the simulated speckle pattern is still 11.84 μm. A series of speckle patterns in different observation planes, i.e., for $0\,\text{mm} \le \varepsilon \le 30\,\text{mm}$, are simulated. Once again, as in the lateral correlation case, the simulated images are resized to maintain the sample interval. The longitudinal correlation coefficients for four different SOP positions $\{(0,0), (1.184\,\text{mm}, 0), (2.368\,\text{mm}, 0), \text{and } (3.552\,\text{mm}, 0)\}$ are provided and compared with the corresponding analytic predictions, for the plane wave see Fig. 4(a), and for Gaussian illumination see Fig. 4(b).

Examining the results plotted in Figs. 3 and 4, for both lateral and longitudinal speckle decorrelation, some differences can be seen between the numerically calculated correlation coefficients and the analytic predictions. However, the decorrelation trends agree quite well as do the positions of the maximum correlation values. Therefore, the relatively small absolute disagreements between the numerical results and the analytic predictions in Figs. 3 and 4 are not of great practical significance. We believe the discrepancies arise mainly due to the resampling/interpolating operation on the simulated speckle image. In addition, the discrete speckle intensities are calculated from area samples (pixels), not the ideal point values assumed in the theoretical derivation,

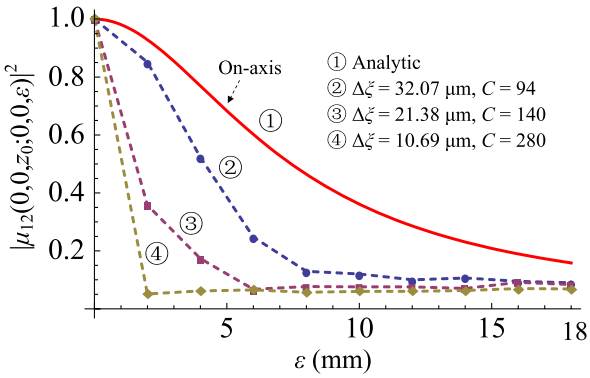

Fig. 6. (Color online) Simulation of longitudinal on-axis decorrelation trend using the SM with different choices of sample interval $\Delta\xi$. (Gaussian beam illumination case).

and we estimate the correlation coefficient value from a "spatial average" around the points of interest. As a result, some disagreements will arise due to the discrepancy between the intensity values used in the simulation and the idealized point values in the theory.

Before proceeding we first wish to examine the use of the SM for speckle field simulation, examining the simulated on-axis longitudinal decorrelation (see Fig. 6). The parameters used are $z_0 = 200$ mm, $w = 1.5$ mm, and $\lambda = 633$ nm. Since Δx only depends on $\Delta\xi$, we set $N = C$, so no zero padding of the input field data is carried out before simulating the field propagation. Three pairs of $(\Delta\xi, C)$ values are used in the simulations $\{(32.07\,\mu\text{m}, 94), (21.38\,\mu\text{m}, 140), \text{and } (10.69\,\mu\text{m}, 280)\}$. These parameters are chosen to facilitate a direct comparison with the DM results. It is clear in Fig. 6 that the decorrelation rate between the longitudinally displaced speckle images is affected by the choice of $\Delta\xi$, and hence cannot be used to safely model the 3D free-space characteristics of speckle fields.

In the SM algorithm implementation first a FFT is applied to the input speckle field, followed by a distance dependent chirp multiplication, and finally an inverse FFT is performed on the result yielding the output Fresnel transformed field. We recall the critical assumption in the analytical treatment of the speckle fields that the autocorrelation of the input distribution is described using a Dirac delta function. This assumption implies that the Fourier transform of the input field is unit valued and broadband (infinite) in the spatial frequency domain. This is not straightforward to represent numerically. The first FFT operation in the implementation of SM leads to a distorted numerical approximation to such a distribution. We therefore conclude that the SM is unsuitable due to the assumption of a delta correlated speckle fields, see [36]. Further work is needed to fully explore the differences between DM- and SM-based speckle simulations, and we note that it may be possible to modify the SM to overcome these difficulties. Here we present some simulation results for SM mainly with the aim of raising the readers' awareness of these serious issues.

4. CONCLUSION

The physical model used to describe the statistical properties of fully developed static speckle in free space has been reviewed. A numerical technique involving the DM approach is provided to simulate the physical predictions. The use of spatial averaging, instead of ensemble averaging, to perform

speckle correlation calculation, has been discussed in detail. In this way the time-consuming realization of the ensemble averaging can be avoided. The discrete correlation coefficients obtained, using the proposed spatial average based correlation algorithm, are shown to be directly comparable to the analytic predictions (calculated using the ensemble average) at each sample position.

This study of the analytic space cross-correlation function of speckle has revealed two important properties: (i) the longitudinal correlation coefficients of two longitudinally displaced speckle patterns decrease monotonically along the radial direction away from the system optical axis and (ii) position shifting of the peak coefficient is observed when an off-axis speckle points field is correlated with the fields from a longitudinally displaced plane.

In Part II [21], the prediction of the model are verified against experimental results for both lateral and longitudinal speckle decorrelations and on- and off-axis cases.

ACKNOWLEDGMENTS

D. Li is supported by a University College Dublin–China Scholarship Council joint scholarship. We also acknowledge the support of the Science Foundation Ireland under the National Development Plan. D. P. Kelly is a Junior-Stiftungs professor of "Optik Design" and is supported by funding from Carl-Zeiss-Stiftung.

REFERENCES

1. J. Ohtsubo, "The second-order statistics of speckle patterns," J. Opt. **12**, 129–142 (1981).
2. T. Yoshimura, "Statistical properties of dynamic speckles," J. Opt. Soc. Am. **3**, 1032–1054 (1986).
3. L. Leushacke and M. Kirchner, "Three-dimensional correlation coefficient of speckle intensity for rectangular and circular apertures," J. Opt. Soc. Am. **7**, 827–832 (1990).
4. Q. B. Li and F. P. Chiang, "Three-dimensional dimension of laser speckle," Appl. Opt. **31**, 6287–6291 (1992).
5. T. Yoshimura and S. Iwamoto, "Dynamic properties of three-dimensional speckles," J. Opt. Soc. Am. **10**, 324–328 (1993).
6. H. T. Yura, S. G. Hanson, R. S. Hansen, and B. Rose, "Three-dimensional speckle dynamics in paraxial optical systems," J. Opt. Soc. Am. **16**, 1402–1412 (1999).
7. D. P. Kelly, J. E. Ward, B. M. Hennelly, U. Gopinathan, F. T. O'Neill, and J. T. Sheridan, "Paraxial speckle-based metrology system with an aperture," J. Opt. Soc. Am. **23**, 2861–2870 (2006).
8. D. P. Kelly, J. E. Ward, U. Gopinathan, B. M. Hennelly, F. T. O'Neill, and J. T. Sheridan, "Generalized Yamaguchi correlation factor for coherent quadratic phase speckle metrology systems with an aperture," Opt. Lett. **31**, 3444–3446 (2006).
9. D. Duncan and S. Kirkpatrick, "Performance analysis of a maximum-likelihood speckle motion estimator," Opt. Express **10**, 927–941 (2002).
10. R. F. Patten, B. M. Hennelly, D. P. Kelly, F. T. O'Neill, Y. Liu, and J. T. Sheridan, "Speckle photography: mixed domain fractional Fourier motion detection," Opt. Lett. **31**, 32–34 (2006).
11. D. P. Kelly, J. E. Ward, U. Gopinathan, and J. T. Sheridan, "Controlling speckle using lenses and free space," Opt. Lett. **32**, 3394–3396 (2007).
12. S. G. Hanson, W. Wang, M. L. Jakobsen, and M. Takeda, "Coherence and polarization of electromagnetic beams modulated by random phase screens and their changes through complex ABCD optical systems," J. Opt. Soc. Am. **25**, 2338–2346 (2008).
13. J. E. Ward, D. P. Kelly, and J. T. Sheridan, "Three-dimensional speckle size in generalized optical systems with limiting apertures," J. Opt. Soc. Am. **26**, 1855–1864 (2009).
14. D. N. Naik, T. Ezawa, Y. Miyamoto, and M. Takeda, "Real-time coherence holography," Opt. Express **18**, 13782–13787 (2010).
15. N. Chang, N. George, and W. Chi, "Wavelength decorrelation of speckle in propagation through a thick diffuser," J. Opt. Soc. Am. **28**, 245–254 (2011).
16. G. P. Weigelt and B. Stoffregen, "The longitudinal correlation of three-dimensional speckle intensity distribution," Optik **48**, 399–408 (1977).
17. C. E. Halford, W. L. Gamble, and N. George, "Experimental investigation of the longitudinal characteristics of laser speckle," Opt. Eng. **26**, 1263–1264 (1987).
18. J. W. Goodman, *Speckle Phenomena in Optics: Theory and Applications*, 1st ed. (Roberts, 2007).
19. I. Yamaguchi, "Speckle displacement and decorrelation in the diffraction and image fields for small object deformation," Opt. Acta **28**, 1359–1376 (1981).
20. D. W. Li and F. P. Chiang, "Decorrelation functions in laser speckle photography," J. Opt. Soc. Am. **3**, 1023–1031 (1986).
21. D. Li, D. P. Kelly, and J. T. Sheridan "Three-dimensional static speckle fields: part II. Experimental investigation," J. Opt. Soc. Am. A **28**, 1904–1908 (2011).
22. G. W. Goodman, "Role of coherence concepts in the study of speckle," Proc. SPIE **194**, 86–94 (1979).
23. D. N. Naik, R. K. Singh, T. Ezawa, Y. Miyamoto, and M. Takeda, "Photon correlation holography," Opt. Express **19**, 1408–1421 (2011).
24. X. Zhao and Z. Gao, "Surface roughness measurement using spatial-average analysis of objective speckle pattern in specular direction," Opt. Lasers Eng. **47**, 1307–1316 (2009).
25. A. Gatti, D. Magatti, and F. Ferri, "Three-dimensional coherence of light speckles: theory," Phys. Rev. **78**, 063806 (2008).
26. D. Magatti, A. Gatti, and F. Ferri, "Three-dimensional coherence of light speckles: experiment," Phys. Rev. **79**, 053831 (2009).
27. D. Mas, J. Garcia, C. Ferreira, L. M. Bernardo, and F. Marinho, "Fast algorithms for free-space diffraction patterns calculation," Opt. Commun. **164**, 233–245 (1999).
28. U. Schnars and W. Jueptner, *Digital Holography: Digital Hologram Recording, Numerical Reconstruction, and Related Techniques*, 1st ed. (Springer, 2004).
29. D. P. Kelly, B. M. Hennelly, W. T. Rhodes, and J. T. Sheridan, "Analytical and numerical analysis of linear optical systems," Opt. Eng. **45**, 088201 (2006).
30. H. M. Pedersen, "Intensity correlation metrology: a comparative study," Opt. Acta **29**, 105–118 (1982).
31. I. S. Reed, "On a moment theorem for complex Gaussian processes," IEEE Trans. Inf. Theory **8**, 194–195 (1962).
32. J. W. Goodman, *Introduction to Fourier Optics*, 3rd ed. (Roberts, 2005).
33. H. Kogelnik and T. Li, "Laser beams and resonators," Proc. IEEE 54, 1312–1329 (1966).
34. MathWorks, http://www.mathworks.com/help/toolbox/images/ref/normxcorr2.html.
35. MathWorks, http://www.mathworks.com/help/toolbox/images/ref/imresize.html.
36. D. P. Kelly, N. Sabitov, T. Meinecke, and S. Sinzinger, "Some considerations when numerically calculating diffraction patterns," in *Digital Holography and Three-Dimensional Imaging*, Technical Digest (CD) (Optical Society of America, 2011), paper DTuC5.